Canyon of current suppression in an interacting two-level quantum dot

Karlström, Olov; Pedersen, Jonas; Samuelsson, Peter; Wacker, Andreas

Published in:
Physical Review B (Condensed Matter and Materials Physics)

DOI:
10.1103/PhysRevB.83.205412

2011

Canyon of current suppression in an interacting two-level quantum dot

O. Karlström, J. N. Pedersen,* P. Samuelsson, and A. Wacker
Mathematical Physics, University of Lund, Box 118, 22100 Lund, Sweden
(Received 5 November 2010; revised manuscript received 18 March 2011; published 18 May 2011)

Motivated by the recent discovery of a canyon of conductance suppression in a two-level equal-spin quantum dot system [Phys. Rev. Lett. **104**, 186804 (2010)], the transport through this system is studied in detail. At low bias and low temperature a strong current suppression is found around the electron-hole symmetry point independent of the couplings, in agreement with previous results. By means of a Schrieffer–Wolff transformation we are able to give an intuitive explanation to this suppression in the low-energy regime. In the general situation, numerical simulations are carried out using quantum rate equations. The simulations allow for the prediction of how the suppression is affected by the couplings, the charging energy, the position of the energy levels, the applied bias, and the temperature. We find that, away from electron-hole symmetry, the parity of the couplings is essential for the current suppression. It is also shown how broadening, interference, and a finite interaction energy cause a shift of the current minimum away from degeneracy. Finally we see how an increased population of the upper level leads to current peaks on each side of the suppression line. At sufficiently high bias we discover a coherence-induced population inversion.

DOI: 10.1103/PhysRevB.83.205412 PACS number(s): 73.63.Kv, 73.23.Hk

I. INTRODUCTION

The conductance of quantum dots is dominated by their discrete-level spectra.[1,2] Particularly interesting features can be found at degeneracies of the discrete levels.[3–5] At zero magnetic field, spin-degenerate levels can be modeled with the Anderson Hamiltonian.[6] At low temperatures, such systems exhibit the intriguing phenomenon of the Kondo effect, which has been extensively investigated.[7] On the contrary, much less is known about systems with orbital degeneracies. The simplest system with such degeneracies is the two-level spinless quantum dot, which was studied theoretically in connection with phenomena such as phase lapses of the transmission phase,[8–10] charge oscillations,[11,12] and correlation-induced conduction resonances.[13] Relations between these phenomena were discussed in Refs. 14 and 15. While Refs. 8–15, investigated the properties of the system in the low-bias limit, this paper deals with the effects of finite bias and temperature. For typical parameters applicable to experiments, we find that changing the bias might lead to qualitatively very different results. Finite bias was previously investigated in Ref. 16, where the current and full counting statistics for the system were studied, but only to lowest order in lead-dot coupling. The effect of finite bias and temperature in the cotunneling regime has thus not previously been investigated. A two-level quantum dot system, where the two levels were coupled to separate source and drain contacts, were studied in a recent paper.[17] Here the orbital quantum number has the same effect as spin, because of the separate contacts, and the orbital Kondo effect can be investigated. The paper studied the level renormalization, Kondo temperature, local density of states, and conductance of the system.

On the experimental side, the degeneracy of orbital levels was recently studied for a gate-defined quantum dot in an InSb nanowire,[18] where a canyon of conductance suppression was found. Here large level-dependent g-factors enabled the study of degenerate orbital levels using the Zeeman effect.[19] Similar systems of quantum dots embedded in nanowires have previously been experimentally realized.[20–22] The model is not restricted to the two-level quantum dot but can also be applied to parallel quantum dots coupled to the same leads.[23–25]

Previous theoretical investigations of the equal-spin two-level quantum dot showed the existence of complete conductance suppression around the electron-hole symmetry point in the limit of zero temperature.[13–15,26] In this paper we investigate the current suppression at finite bias and temperature, as well as the current away from electron-hole symmetry, i.e., regimes not previously studied beyond sequential tunneling. The aim of this paper is to determine whether the canyon of current suppression is generic or appears only for certain parameters. In the regime $\Gamma > V_{\rm bias}, k_B T$, where Γ is the level broadening given by the coupling between dot levels and leads, we find a complete current suppression close to degeneracy, in both the cotunneling and the sequential-tunneling regime, assuming that the two dot states couple to the leads with different parity. For weaker couplings to the leads, or for increased $V_{\rm bias}$ or $k_B T$, only partial current suppression is found. Results are compared with three limiting cases of bias: (i) The low-bias limit, $V_{\rm bias} < \Gamma, U$, is shown in Fig. 1(a), where U is the charging energy; (ii) the high-bias limit $\Gamma, \Delta E < V_{\rm bias} < U$, see Fig. 1(b), where ΔE is the splitting between the two levels, so that both E_1 and E_2 are entirely inside the bias window; and (iii) the ultra-high bias in which the bias is the largest parameter $\Gamma, \Delta E, U < V_{\rm bias}$, as shown in Fig. 1(c).

For the high-bias and ultra-high-bias limits the current can be evaluated by analytical means, as first-order approximations in tunneling are valid. We find that, in the high-bias limit, the current suppression is completely independent of the couplings.[27,28] In the ultra-high-bias limit, on the other hand, only partial suppression is found when the two states have different coupling strengths to the leads.

The remainder of the article is organized as follows. The system Hamiltonian and the modeling of transport is discussed in Sec. II. The canyon of current suppression is studied in Sec. III using the second-order von Neumann (2vN) method, where cotunneling and coherence are included.[29] The findings

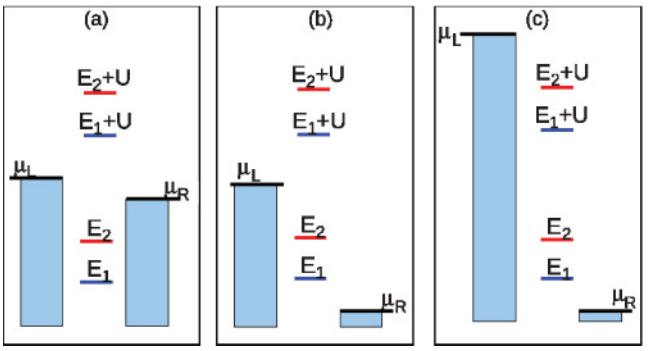

FIG. 1. (Color online) Level configuration at (a) low bias, (b) high bias, and (c) ultra-high bias. Because of the Coulomb interaction the energies of the levels are increased by an amount U when the other state is filled. The applied bias is given by $\mu_L - \mu_R$, where μ_L and μ_R are the chemical potentials in the left and right contact, respectively.

of this section are further explained in Secs. IV–VII. In Sec. IV an intuitive explanation for the conductance suppression is given by means of a Schrieffer–Wolff transformation.[30] In Sec. V the current at electron-hole symmetry is analyzed as a function of bias, temperature, and couplings. The current away from electron-hole symmetry is studied in Sec. VI. In Sec. VII the focus is changed to the current peaks surrounding the canyon of current suppression. At increased bias we discover an unexpected population inversion and investigate its importance for the peaks. Here the term population inversion means a higher population of the upper level. It should be pointed out that this population inversion results from a finite bias and is different from what is studied in Refs. 11 and 12.

II. MODELING OF TRANSPORT

In this section we discuss the Hamiltonian of the equal-spin two-level quantum dot as well as the modeling of the current through the system. In the single-particle eigenbasis of the dot, the system Hamiltonian is given by

$$\hat{H} = \hat{H}_{\rm dot} + \hat{H}_{\rm leads} + \hat{H}_T, \tag{1}$$

$$\hat{H}_{\rm dot} = E_1 d_1^\dagger d_1 + E_2 d_2^\dagger d_2 + U d_1^\dagger d_1 d_2^\dagger d_2, \tag{2}$$

$$\hat{H}_{\rm leads} = \sum_{k,\ell=L/R} E_k c_{k\ell}^\dagger c_{k\ell}, \tag{3}$$

$$\hat{H}_T = \sum_{k,\ell=L/R} (t_{\ell 1} d_1^\dagger + t_{\ell 2} d_2^\dagger) c_{k\ell} + \text{H.c.}, \tag{4}$$

where we have assumed that the couplings $t_{\ell i}$ are independent of k and $\Gamma_{\ell i}(E) = 2\pi t_{\ell i}^2 \rho_0$ with a constant density of states $\rho_0(E) = \sum_k \delta(E_k - E)$, for $-D < E_k < D$. In the simulations a large bandwidth D is used, assuming wide conduction bands of the leads. The operators d_i ($d_i^\dagger$) and c_{kl} ($c_{kl}^\dagger$) are annihilation (creation) operators of electrons in the dot and leads, respectively. In Eq. (2) the charging energy U is due to Coulomb interaction between the electrons when both dot states are filled.

The energy levels are parameterized by

$$E_{1/2} = \pm\frac{\Delta E}{2} - E_g - U/2. \tag{5}$$

Electron-hole symmetry, where the levels are symmetrically placed around the Fermi energy, is given by $E_g = 0$ and $\Delta E = 0$. At this point electrons and holes contribute equally to the current through the quantum dot. Bias is applied symmetrically to the quantum dot so that the chemical potentials are $\mu_L = V_{\rm bias}/2$ and $\mu_R = -V_{\rm bias}/2$, for the left and right contact, respectively.

In this paper we mainly study couplings of the type

$$t_{L1} = t, \quad t_{R1} = t, \quad t_{L2} = -at, \quad t_{R2} = at, \tag{6}$$

where the asymmetry parameter a is chosen to be real. Time-reversal symmetry encsures that the coupling elements are real, implying that the two dot states couple to the leads with the same or opposite parity.[9] This paper focuses on the case of opposite parity as it is essential for the canyon of current suppression at finite bias; see Sec. III where also the effects of asymmetric couplings to left and right leads are briefly discussed. Furthermore, it was shown in Ref. 18 that good agreement between theory and experiment could be achieved for real couplings. As the broadening of the levels is proportional to the square of the coupling elements we have $\Gamma_{L1} = \Gamma_{R1} = \Gamma_1, \Gamma_{L2} = \Gamma_{R2} = a^2\Gamma_1$.

The current through the dot is calculated using the 2vN method.[29] This method is an extension of the generalized master equation. Starting from the von Neumann equation, an equation of motion is derived not only for the reduced density matrix but also for the elements of the total density matrix consisting of a single electron-hole excitation in the contact. In the latter system of equations two electron-hole excitation elements, corresponding to cotunneling, enter. In the time evolution of the cotunneling processes there are contributions from three electron-hole excitation elements, but these are ignored. This results in a closed set of equations, which can be solved for the occupations of the dot levels, the coherences between these resulting from the coupling to the leads, and the current flowing through the quantum dot.

There are currently several other methods that account for tunneling of higher order than sequential processes. The most widely used technique is the generalized master equation approach, which can be derived in many different ways including the real-time diagrammatic technique[31,32] and the Bloch–Redfield approach originally developed in Refs. 33–35. Comparisons of different approaches have been performed in Refs. 36 and 37. The detailed relation between these methods and the 2vN method will be the subject of future investigations, where we show that the 2vN method is similar to other methods of fourth order in the couplings t, but contains certain diagrams up to infinite order. For the Anderson model with infinite U it has been shown to give the same current as the resonant-tunneling approximation[38] in the real-time diagrammatic approach.[39] This method includes irreducible diagrams with an arbitrary number of correlated tunneling processes, but is restricted to one electron-hole excitation at any given moment.

III. THE CANYON OF CONDUCTANCE SUPPRESSION

We proceed by investigating whether the canyon of current suppression observed in Ref. 18 can be found only in a certain parameter space or if it is generic for the studied two-level system. We plot the normalized current J/V_{bias}, which equals the conductance G in the low-bias limit. As a start, we restrict ourselves to couplings given by Eqs. (6) and study two different coupling strengths, $\Gamma_1/k_BT = 1$ and $\Gamma_1/k_BT = 4$. In both cases the relative coupling strength of the two levels is given by $a = 0.5$. The reason for using $\Gamma_1 > k_BT$ is that we want to study the current suppression in the cotunneling regime. The complete suppression found close to degeneracy in the case of $\Gamma_1/k_BT = 4$ is also supported by the analytical arguments of Sec. IV. Furthermore the 2vN method is nonperturbative and contains some classes of diagrams up to infinite order, which makes the analysis in the regime $\Gamma > k_BT$ more reliable. Both low bias $V_{\text{bias}}/k_BT = 1$ and high bias $V_{\text{bias}}/k_BT = 15$ are studied to investigate the effects of finite bias. In the left part of Fig. 2, the results of the 2vN simulations for $U/k_BT = 25$ are shown. To study the role of the Coulomb interaction, corresponding results for $U = 0$ are shown in the right part of Fig. 2. Here we applied the method of nonequilibrium Green's functions (NEGFs),[9,40] providing identical results to the numerically much more involved 2vN method (for $U = 0$), for the simple system studied here. We believe that this holds also for more complex systems; see also Refs. 29 and 41.

To facilitate the comparison, we performed a cut of the noninteracting results at $E_g = 0$ and shifted the upper and lower parts by $\pm 12.5\,k_BT$. This mimics the presence of Coulomb repulsion by one entirely filled or completely empty level, as expected in the respective energy range. Plotting the noninteracting results in this way we find indeed rather good agreement with the interacting results in the low-bias regime, allowing us to explain the essential features in this region. For high bias the current suppression is more pronounced in the interacting case.

The Coulomb blockade regime present in the left figure is a result of the interaction-related correlations. This regime can naturally not be studied using non-interacting methods.

The noninteracting results for weak bias, Figs. 2(b) and 2(d), show a line of current suppression, which is bowed toward the weaker resonance. This can be understood in terms of interference between the two levels. The Breit–Wigner formula provides

$$T(E) = \Gamma_1^2 \left| \frac{1}{E - E_1 + i\Gamma_1} - \frac{a^2}{E - E_2 + ia^2\Gamma_1} \right|^2, \quad (7)$$

and the current can then be calculated using

$$J = \frac{1}{h} \int_{-\infty}^{\infty} [f_L(E) - f_R(E)] T(E)\, dE. \quad (8)$$

Vanishing conductance in the low-temperature limit corresponds to $T(0) = 0$, i.e., complete conductance suppression can occur only for $E_2 = a^2 E_1$. This explains the location of the strong current suppression found in Figs. 2(b) and 2(d). It is easily shown that if one level couples symmetrically to left

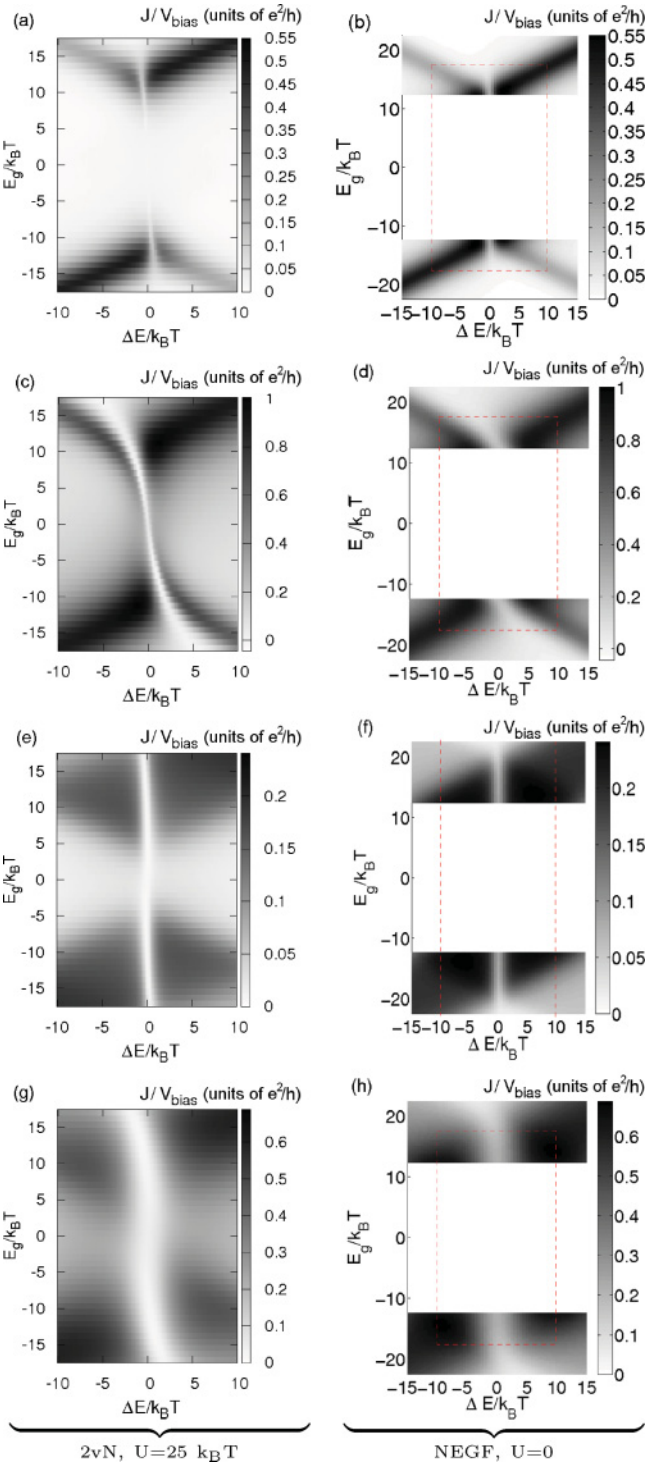

FIG. 2. Conductance calculated with the 2vN method for the interacting system, $U = 25\,k_BT$ to the left, and the noninteracting Green's function result to the right. The white areas in the right figures are the regions where the noninteracting formalism is not valid. The upper four figures correspond to the low-bias limit $V_{\text{bias}} = k_BT$, while the lower four show the results for high bias $V_{\text{bias}} = 15\,k_BT$. The couplings are given by Eqs. (6) with $\Gamma_1 = k_BT$ and $a = 0.5$ for figures (a), (b), (e), and (f), while $\Gamma_1 = 4\,k_BT$ and $a = 0.5$ for figures (c), (d), (g), and (h). The dashed boxes in the noninteracting figures mark the studied region in the interacting case.

and right, complete suppression is found only for couplings like Eqs. (6), where the sign of t_{Li} and t_{Ri} differs for $i = 1,2$. This motivates the special attention given to these couplings.

As the bias is increased the current not only depends on $T(0)$. When the bias is larger than the width of the dip, $a\Gamma_1$ at $E_1 = E_2 = 0$ resulting from Eq. (7), this results in only partial current suppression, as can be seen in Figs. 2(f) and 2(h).

Figure 2(a) shows that the weak coupling and low-bias interacting result are well reproduced by the noninteracting result, Fig. 2(b), in its region of applicability ($|E_g| > U/2$), apart from a slight shift of the suppression line. In the Coulomb blockade regime ($|E_g| < U/2$) almost no structure is visible because of the very weak cotunneling. In Sec. V we see that this corresponds to the regime where k_BT dominates and only partial conductance suppression can be found.

Figure 2(c) shows that the 2vN method can sometimes give unphysical results corresponding to small negative currents. This is expected as the 2vN method neglects some correlated transitions of more than two electrons or holes. The contributions of these terms become important in the limit of large couplings and small temperature and bias. Apart from this, the 2vN method agrees well with the noninteracting results. However, we see that the shift of the suppression line is larger when the couplings are strong. As explained in Sec. VI this can be attributed to the broadening of the levels. In the Coulomb blockade regime a clear conductance suppression is found. This is the regime where Γ dominates, i.e., the situation described by Refs. 13–15.

In the high-bias limit, the interacting and noninteracting results differ significantly at the canyon of current suppression, as seen in Figs. 2(d), 2(g), 2(f), and 2(h), respectively. In the sequential tunneling regime a strong current suppression is found in the interacting case. This result has been explained by Refs. 27 and 28 and is further discussed in Sec. VI. This interaction-induced suppression is not included in the NEGF method, resulting in only partial suppression, as can be seen from the gray-colored canyon.

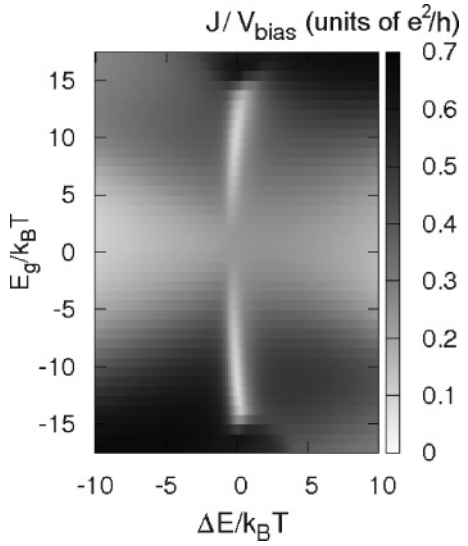

FIG. 3. Conductance calculated with the 2vN method. The two levels have equal parity with couplings given by $t_{L1} = t_{R1} = t$, $t_{L2} = 0.4t$ and $t_{R2} = 0.6t$ with $\Gamma_{L1} = \Gamma_{R1} = 2\pi\rho_0 t^2 = 5\,k_BT$. Additional parameters are $V_{\text{bias}} = 15\,k_BT$, $U = 25\,k_BT$.

TABLE I. A summary of the current suppression from Fig. 2. For levels with couplings of different parity the current suppression is generic, but not always complete. The high-bias limit of Fig. 1(b) implies that $E_g \approx \pm U/2$. Therefore the cotunneling regime is not applicable (n.a.) in this limit. In the ultra-high-bias limit the current is given by the sequential-tunneling result. The cotunneling regime is thus not categorized in this limit. The table also indicates in which sections the different regimes are investigated further.

Γ	V_{bias}	Cotunneling ($E_g \approx 0$)	Sequential Tunneling ($E_g \approx \pm U/2$)
$>k_BT$	Low	Complete (Secs. IV and V)	Complete (Sec. VI)
$>k_BT$	High	n.a.	Complete (Sec. VI)
$>k_BT$	Ultra-high	–	Partial (Sec. V)
$<k_BT$	Low	Partial (Sec. V)	Partial (Sec. VI)
$<k_BT$	High	n.a.	Complete (Sec. VI)
$<k_BT$	Ultra-high	–	Partial (Sec. V)

The current suppression in the cotunneling region becomes weaker as we are approaching the region where V_{bias} dominates, which results in only partial current suppression, see Sec. V. This shows that the canyon of current suppression is found in all four cases, albeit the current does not always entirely drop to zero. Further investigations show that the canyon of suppression is not restricted to couplings like Eqs. (6), but is present also for couplings that are asymmetric with respect to the left and right contact. The importance of the relative coupling strength a is investigated in Sec. V.

For couplings where the two levels have the same parity, i.e., the two levels couple with the same sign to left and right leads, the situation is different, as shown in Fig. 3. Here we still see the high-bias blockade in the sequential-tunneling regime.[27,28] For $E_g < -U/2$ or $E_g > U/2$ interactions are of less importance and the blockade disappears. One also sees that no canyon is visible in the Coulomb blockade regime. The reason is that the width of the dip in the transmission function becomes increasingly narrow as the singular coupling point is approached. At such couplings, one can at degeneracy completely decouple one level from the leads, resulting in a bistable system; see also Refs. 13 and 14. As a result, the canyon is present only for very low bias and temperature, i.e., a regime where the 2vN method is not applicable. Figure 3 clearly shows that at finite bias the parity of the couplings is essential for the suppression, unlike the zero-bias limit. Two levels with the same parity will not be studied any further. The remainder of the paper is devoted to the couplings described by Eqs. (6). For such couplings, details of the canyon of current suppression is summarized in Table I, which can be of use for futher experimental studies.

IV. TUNNELING PROCESSES IN THE LOW-ENERGY LIMIT

In this section we study the current in the regime where $E_1, E_2 < 0$ and $E_1 + U, E_2 + U > 0$, so that the dot is singly occupied. Furthermore we assume that $V_{\text{bias}}, k_BT \to 0$. This allows us to derive an effective low-energy Hamiltonian by means of a Schrieffer–Wolff transformation. Low energy

implies that all tunneling events occur around $E_k = 0$. The transformation requires that the charging energy of the dot be much larger than the broadening of the dot levels, so that the dot is singly occupied when the levels are placed as in Fig. 1(a). By analyzing the effective Hamiltonian in this regime we will be able to identify the two-particle processes contributing to the current and give an intuitive explanation of the conductance suppression. It is convenient to write the Hamiltonian in terms of pseudospin operators[14,15] defined by $d_\uparrow = d_1$, $d_\downarrow = d_2$, $c_{k\uparrow} = (c_{kL} + c_{kR})/\sqrt{2}$, and $c_{k\downarrow} = (-c_{kL} + c_{kR})/\sqrt{2}$. The system Hamiltonian then reads

$$\hat{H}_{\rm dot} = E_\uparrow d_\uparrow^\dagger d_\uparrow + E_\downarrow d_\downarrow^\dagger d_\downarrow + U d_\uparrow^\dagger d_\uparrow d_\downarrow^\dagger d_\downarrow, \tag{9}$$

$$\hat{H}_{\rm leads} = \sum_{k,\sigma=\uparrow/\downarrow} E_k c_{k\sigma}^\dagger c_{k\sigma}, \tag{10}$$

$$\begin{aligned}\hat{H}_T &= \sum_{\sigma k} t_\sigma c_{k\sigma}^\dagger d_\sigma + \text{H.c.} \\ &= \sum_k \sqrt{2} t (c_{k\uparrow}^\dagger d_\uparrow + a c_{k\downarrow}^\dagger d_\downarrow) + \text{H.c.}\end{aligned} \tag{11}$$

Here $E_\uparrow = E_1$, $E_\downarrow = E_2$, $t_\uparrow = \sqrt{2}t$, $t_\downarrow = \sqrt{2}at$, and the problem has been mapped onto the one-lead Anderson model with spin-dependent couplings. A similar transformation can be found for arbitrary couplings.

We now perform a Schrieffer–Wolff transformation, i.e., a canonical transformation,

$$\hat{H}_S = e^{iS} \hat{H} e^{-iS}, \tag{12}$$

so that $\hat{H}_S$ does not have a linear term in $\hat{H}_T$. We find that the following transformation $S = S^+ + S^-$, with

$$\begin{aligned}S^- = -i \sum_{\sigma k} \Bigg(&\frac{t_\sigma}{E_k - (E_\sigma + U)} n_{\bar\sigma} c_{k\sigma}^\dagger d_\sigma \\ &+ \frac{t_\sigma}{E_k - E_\sigma} (1 - n_{\bar\sigma}) c_{k\sigma}^\dagger d_\sigma \Bigg),\end{aligned} \tag{13}$$

and $S^+ = (S^-)^\dagger$, will do the job. Here $\overline{\sigma} = \downarrow$ if $\sigma = \uparrow$ and $\overline{\sigma} = \uparrow$ if $\sigma = \downarrow$. Writing the tunneling Hamiltonian as $\hat{H}_T = \hat{H}_T^+ + \hat{H}_T^-$, with

$$\hat{H}_T^- = \sum_{\sigma k} t_\sigma c_{k\sigma}^\dagger d_\sigma, \tag{14}$$

and $\hat{H}_T^+ = (\hat{H}_T^-)^\dagger$, the effective low-energy Hamiltonian of the singly occupied subspace, when restricted to two-particle tunneling, is given by

$$\begin{aligned}\hat{H}_S = \; &\hat{H}_{\rm dot} + \hat{H}_{\rm leads} \\ &+ \underbrace{\frac{i}{2}([S^-, \hat{H}_T^+] + [S^+, \hat{H}_T^-])}_{\hat{H}_{TS}} + O(\hat{H}_T^3),\end{aligned} \tag{15}$$

where the last term is the effective tunneling Hamiltonian $\hat{H}_{TS}$. Performing the commutations and returning to our original basis we find

$$\begin{aligned}\hat{H}_{TS} = \; &\frac{1}{2} \overline{\sum_{kk'}} \left(\frac{t^2 d_2^\dagger d_2}{E_k - (E_1 + U)} + \frac{t^2 (1 - d_2^\dagger d_2)}{E_k - E_1} \right) (c_{kL}^\dagger + c_{kR}^\dagger)(c_{k'L} + c_{k'R}) \\ &+ \frac{1}{2} \overline{\sum_{kk'}} \left(\frac{a^2 t^2 d_1^\dagger d_1}{E_k - (E_2 + U)} + \frac{a^2 t^2 (1 - d_1^\dagger d_1)}{E_k - E_2} \right) (c_{kL}^\dagger - c_{kR}^\dagger)(c_{k'L} - c_{k'R}) \\ &+ \frac{1}{2} \sum_{kk'} \left(\frac{at^2}{E_k - (E_1 + U)} - \frac{at^2}{E_k - E_1} \right) (c_{kL}^\dagger + c_{kR}^\dagger)(c_{k'L} - c_{k'R}) d_2^\dagger d_1 \\ &+ \frac{1}{2} \sum_{kk'} \left(\frac{at^2}{E_k - (E_2 + U)} - \frac{at^2}{E_k - E_2} \right) (c_{kL}^\dagger - c_{kR}^\dagger)(c_{k'L} + c_{k'R}) d_1^\dagger d_2 \\ &+ \text{H.c.} + \hat{H}_{\rm renorm},\end{aligned} \tag{16}$$

where $\overline{\sum}$ indicates that the terms containing $c_{kL}^\dagger c_{kL} + c_{kR}^\dagger c_{kR}$, corresponding to the renormalization of energy levels $H_{\rm renorm}$, are not included in the sum. In the limit of zero temperature and zero bias, the renormalization reads (see Appendix B)

$$\hat{H}_{\rm renorm} = \frac{\Gamma_1}{\pi} \left(\ln \left| \frac{E_1}{E_1 + U} \right| d_1^\dagger d_1 + a^2 \ln \left| \frac{E_2}{E_2 + U} \right| d_2^\dagger d_2 \right). \tag{17}$$

It should be noted that the above expression does not hold if one of the levels is close to the chemical potential, as the Schrieffer–Wolff transform breaks down in this regime. The effect of the renormalization will be further discussed in Sec. V; here we simply note that at electron-hole symmetry, where $E_1 = E_2 = -U/2$, the renormalization vanishes.

Each term in Eq. (16) corresponds to a cotunneling process, where the electron is transferred from one lead to the other, or returns to the original lead. The first two sums correspond to elastic processes where the state of the dot is unchanged. The next two sums correspond to inelastic processes where the state of the dot changes.

Generally there is an effective overlap matrix element between the two dot states originating from the coupling to the leads. In Refs. 26 and 42 it was shown that, for couplings of the type in Eqs. (6), this overlap vanishes. Indeed,

evaluating the $k = k'$ inelastic terms in Eq. (16) results in factors $c_{kL}^\dagger c_{kL} - c_{kR}^\dagger c_{kR} = 0$ in the low-bias limit; see Sec. VII for a discussion concerning finite bias.

Let us now analyze Eq. (16) in detail: We see that only the inelastic processes affect the occupations of the dot, as $d_1^\dagger d_1$ and $d_2^\dagger d_2$ commutes with the other parts of $\hat{H}_{TS}$. For $E_1 = E_2$ the third and fourth sum in Eq. (16), corresponding to the inelastic processes, are symmetric in levels 1 and 2 except for a sign change $\mp c_{kL}^\dagger c_{k'R} \pm c_{kR}^\dagger c_{k'L}$. In the low-bias limit, this sign change does not affect the kinetics of the occupations and we conclude that both levels are half filled at degeneracy.

The current operator reads $\hat{J}_S = -\sum_k \frac{i}{\hbar}[\hat{H}_S, c_k^\dagger c_k]$, resulting in

$$\hat{J}_S = -\frac{it^2}{2\hbar}\sum_{kk'}\left(\frac{d_2^\dagger d_2}{E_k - (E_1+U)} + \frac{d_1^\dagger d_1}{E_k - E_1} - \frac{a^2 d_1^\dagger d_1}{E_k - (E_2+U)} - \frac{a^2 d_2^\dagger d_2}{E_k - E_2}\right)(c_{kR}^\dagger c_{k'L} - c_{kL}^\dagger c_{k'R})$$
$$- \frac{iat^2}{\hbar}\sum_{kk'}\left[\left(\frac{1}{E_k - (E_1+U)} - \frac{1}{E_k - E_1}\right)d_2^\dagger d_1 - \left(\frac{1}{E_k - (E_2+U)} - \frac{1}{E_k - E_2}\right)d_1^\dagger d_2\right](c_{kR}^\dagger c_{k'L} + c_{kL}^\dagger c_{k'R}) + \text{H.c.}, \tag{18}$$

where $d_1^\dagger d_1 + d_2^\dagger d_2 = 1$ has again been used. The first row corresponds to elastic processes, while the second row constitutes the inelastic processes. We adopt the notation $|0\rangle$, $|1\rangle$, $|2\rangle$, and $|d\rangle$, corresponding to the dot being empty, in state 1, in state 2, or doubly occupied. The term $d_2^\dagger d_2/(E_k - (E_1 + U))$ represents the elastic processes $|2\rangle \to |d\rangle \to |2\rangle$. The denominator includes the energy difference between the two states involved in the process, $E_d - E_2 = E_1 + E_2 + U - E_2 = E_1 + U$, and the numerator represents the fact that state $|2\rangle$ has to be occupied for this process to occur. In the same way the term $d_1^\dagger d_1/(E_k - E_1)$ represents the process $|1\rangle \to |0\rangle \to |1\rangle$. Assuming $E_k = 0$, corresponding to low bias and low temperature, we see that these terms cancel completely at the electron-hole symmetry point $E_1 = E_2 = -U/2$, owing to the equal population of the two levels. We note that these two processes, involving tunneling into and out of state $|1\rangle$, use the couplings of this state. In the same way we see how the two processes $|1\rangle \to |d\rangle \to |1\rangle$ and $|2\rangle \to |0\rangle \to |2\rangle$ cancel. The factor of a^2 enters here as it is state $|2\rangle$ that is active in these processes. We have seen that the elastic cotunneling processes cancel completely at the electron-hole symmetry point, independent of the relative coupling strength of the two levels. Away from electron-hole symmetry, we see that the processes no longer cancel. However, at $E_1 = E_2$, we again find complete canceling for $a = 1$.

We now investigate the inelastic processes. It can easily be seen that the terms involving $d_2^\dagger d_1$ and $d_1^\dagger d_2$ cancel at $E_1 = E_2$ because of the equal occupation of the two levels. Electron-hole symmetry is thus not required for the canceling of the inelastic terms; degeneracy of the two levels is sufficient.

To summarize we have shown that at $E_1 = E_2 = -U/2$ the current suppression is complete in the limit of low bias and low temperature at the electron-hole symmetric point. Unlike previous explanations of this phenomena our derivation gives an intuitive explanation to the suppression in terms of canceling of cotunneling processes. It also explains why the suppression is not complete for finite bias and temperature or away from electron-hole symmetry. This will be further studied in Secs. V and VI, respectively. The suppression is not an interference effect between different processes, since the processes that cancel involve different initial and final states. The processes instead cancel as a result of the equal population of the two levels. At degeneracy, but away from electron-hole symmetry, the elastic processes do not cancel unless $a = 1$. There is, however, partial canceling due to the different parity of the two levels. We stress that the complete suppression at electron-hole symmetry is not an effect of this difference in parity. The pseudospin operators are always orthogonal. It is this orthogonality that gives equal occupations of the two levels and ensures the canceling of current-carrying processes in the low-bias limit. The canceling is due to the phase lapse between the elastic cotunneling processes using $|0\rangle$ and $|d\rangle$ as the virtual intermediate state. This shows the relationship among population switches, phase lapses, and vanishing conductance, which was previously investigated in Ref. 14. At electron-hole symmetry the vanishing conductance is thus an effect of the correlations induced by the Coulomb interaction.

V. CURRENT SUPPRESSION AT ELECTRON-HOLE SYMMETRY

In the previous section we saw that the current suppression was most pronounced at the electron-hole symmetry point. In this section we will investigate the suppression at this point in more detail. The current is calculated as the flow of particles from the left contact into the dot. Because of current conservation this is, in the stationary case, of course equal to the current flowing from the dot into the right contact. Thus we do not label the current with any lead index. To quantify the extent of the current suppression we introduce the dimensionless ratio between the current through the two-level dot corresponding to Eq. (2) and the current through a single-level dot containing only level 1:

$$Q = \frac{J_{\text{both levels}}}{J_{\text{level 1}}}. \tag{19}$$

This ratio measures how much the presence of level 2 suppresses the current. In the regime where sequential tunneling is dominating the first order-von Neumann (1vN) method can be used to approximately evaluate the current; see Appendix A. Using the couplings of Eqs. (6), it is possible to derive Eq. (A8). At electron-hole symmetry, $E_1 = E_2 = -U/2$, this simplifies to

$$\begin{aligned} J = \frac{\Gamma_1}{\hbar}\{&w_{00} f_L(-U/2)(1+a^2) - w_{11}[1 - f_L(-U/2)] \\ &+ w_{11} f_L(U/2)a^2 - w_{22}[1 - f_L(-U/2)]a^2 \\ &+ w_{22} f_L(U/2) - w_{dd}[1 - f_L(U/2)](1+a^2) \\ &+ 2a\mathcal{R}\{w_{12}\}[1 - f_L(-U/2) + f_L(U/2)]\}, \end{aligned} \tag{20}$$

where w_{00}, w_{11}, w_{22} and w_{dd} are the probabilities of finding the dot empty in state 1, in state 2, and doubly occupied, respectively, while w_{12} is the coherence between level 1 and 2. Here $\mathcal{R}$ denotes the real part. In this paper we refer to the coherence as the nondiagonal elements of the reduced density matrix. The coherence is thus a basis-dependent quantity. The first terms of Eq. (20) are identical to the corresponding Pauli master equation and are easily interpreted in terms of transition rates. The last term originating from the coherence of the two levels is more difficult to understand intuitively. However, it is evident that a negative real part of the coherence results in a decreased current.

At level degeneracy we can get rid of the coherence term by performing a basis change that diagonalizes the reduced density matrix. Here we focus on the case of electron-hole symmetry, $E_1 = E_2 = -U/2$, where levels 1 and 2 have the same occupation and the coherence is real (see Appendix A). The singly occupied part of the reduced density matrix can thus be written as

$$\begin{pmatrix} w_{11} & w_{12} \\ w_{21} & w_{22} \end{pmatrix} = \begin{pmatrix} w_{11} & w_{12} \\ w_{12} & w_{11} \end{pmatrix} = SDS^{-1}.$$

The diagonalization is given by

$$S = \frac{1}{\sqrt{2}}\begin{pmatrix} 1 & 1 \\ 1 & -1 \end{pmatrix}, \quad D = \begin{pmatrix} w_{11} + w_{12} & 0 \\ 0 & w_{11} - w_{12} \end{pmatrix}$$

where the diagonal elements of D are the occupations in the new basis.

The couplings in the new eigenbasis are given by

$$\begin{aligned} t'_{L1} &= \frac{t}{\sqrt{2}}(1-a), \quad t'_{R1} = \frac{t}{\sqrt{2}}(1+a), \\ t'_{L2} &= \frac{t}{\sqrt{2}}(1+a), \quad t'_{R2} = \frac{t}{\sqrt{2}}(1-a). \end{aligned} \tag{21}$$

In the new basis one level couples strongly to the left, while the other couples strongly to the right lead. This results in a strong current suppression and also explains the occupations in our new basis: The level that is strongly coupled to the lead with a high chemical potential has a high occupation. A high bias thus results in a large coherence between the levels; cf. the expression for the matrix D. For $a = 1$, i.e., both levels have the same coupling strength, each level decouples completely from one lead. As a result no current can flow through the quantum dot; see also Ref. 42. The effect of the coherence is thus to decrease the current. As the coherence is zero in the new basis we can use the Pauli master equation approach to derive the current. At electron-hole symmetry we obtain

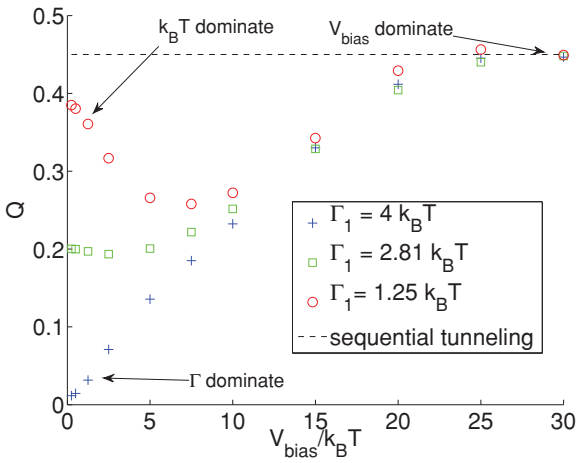

FIG. 4. (Color online) Q as a function of V_{bias} at electron-hole symmetry for different coupling strengths. All curves correspond to $a = 0.5$ and $U = 25\,k_BT$.

$$J_{\text{both levels}} = \frac{(1-a^2)^2\Gamma_1}{2\hbar(1+a^2)}[f_L(-U/2) - f_R(-U/2)]. \tag{22}$$

If only level 1 was present the current would be given by

$$J_{\text{level 1}} = \frac{\Gamma_1}{2\hbar}[f_L(-U/2) - f_R(-U/2)], \tag{23}$$

and the resulting ratio is

$$Q = \frac{J_{\text{both levels}}}{J_{\text{level 1}}} = \frac{(1-a^2)^2}{1+a^2}. \tag{24}$$

This result is valid when sequential tunneling is dominating.

In Fig. 4 the current suppression, Q, at electron-hole symmetry, $E_1 = E_2 = -U/2$, is shown as a function of the applied bias. The numerator of Q is calculated using the 2vN method, while the denominator is calculated using NEGF which, however, agrees exactly with 2vN for the single-level dot. Figure 4 clearly shows that when $V_{\text{bias}} > U$, the ultra-high-bias regime, where sequential tunneling is dominating, is entered and the results of the 2vN simulations agree very well with the analytical results, Eq. (24).

In the low-bias limit the results are more complicated. For weak couplings the contribution from cotunneling processes is small and the first-order result, Eq. (24), is approached. As the bias is increased the phase space for cotunneling processes ($\sim V_{\text{bias}}$) increases, so these can no longer be neglected. This results in a stronger current suppression and a related decrease in Q for the weaker couplings. For strong couplings, i.e., $\Gamma > V_{\text{bias}}, k_BT$, cotunneling dominates and the low-energy Hamiltonian of Sec. IV predicts complete suppression in the low-bias limit. We stress that the suppression in the low-bias limit is not an artifact of neglecting higher-order processes. As was shown in Sec. IV and Refs. 13–15 and 26, the suppression is complete in the limit of low bias and low temperature, at the electron-hole symmetric point.

In Fig. 5 the simulated current suppression at electron-hole symmetry is shown for different temperatures as a function of bias. As the temperature is not constant in Figs. 5 and 6 we here

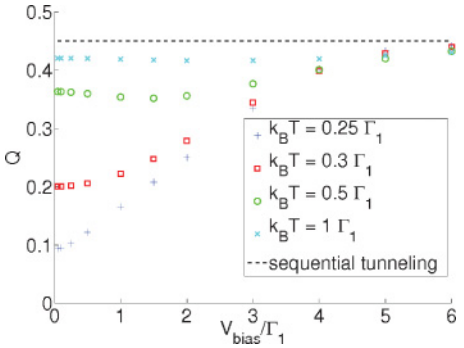

FIG. 5. (Color online) Q as a function of V_{bias} at electron-hole symmetry for different temperatures. All curves correspond to $a = 0.5$ and $U = 5\Gamma_1$.

express all energies in terms of Γ_1. It is clearly seen that the sequential-tunneling result is reached in the high-temperature limit.

In Fig. 6 we investigate the current suppression Q as a function of the difference a in coupling strength between the two levels for different temperatures. For lower temperatures it can be seen that there is essentially complete suppression when both levels have equal coupling strength, i.e., $a \approx 1$. When $a \approx 0$ and the difference in coupling strength is large, almost no suppression is observed. This is expected as no current flows through the weakly coupled state, and because of electron-hole symmetry it does not matter if it is occupied or not.

In this section we investigated how a finite bias and temperature affect the suppression at electron-hole symmetry. In the limits of low and high bias and temperature we compared with previously established results and first-order simulations and found good agreement. In intermediate regimes we found that the current suppression could show a nonmonotonous behavior; see $\Gamma_1 = 1.25\, k_B T$ in Fig. 4. Furthermore Figs. 4, 5, and 6 show that Q increases with increasing temperature until the high-temperature limit is reached. We have seen how the current suppression is given by analytical first-order results in

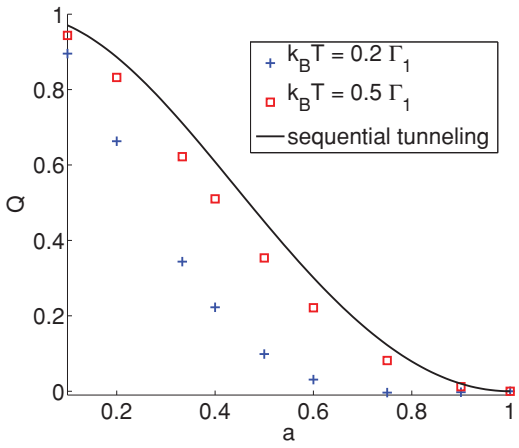

FIG. 6. (Color online) Q as a function of the difference in coupling strength a, see Eqs. (6), at electron-hole symmetry for different temperatures. The high-temperature limit is given by Eq. (24). All curves correspond to $V_{\text{bias}} = 1\Gamma_1$ and $U = 5\Gamma_1$.

the regimes where sequential tunneling is dominating. In this regime the suppression is coherence induced and only partial unless both levels have the same coupling strength. Stronger couplings lead to an increased cotunneling that results in a stronger suppression.

VI. CURRENT SUPPRESSION AWAY FROM ELECTRON-HOLE SYMMETRY

With a clear picture of the current suppression at electron-hole symmetry, we now change focus to the regime away from this symmetry point. We will investigate the current at $E_g = -U/2$. At this point the singly occupied levels are close to the chemical potentials of the leads, and sequential tunneling contributes strongly to the transport. Thus the 1vN-method gives reasonable results and we can compare 1vN and 2vN methods to investigate the importance of the broadening in this regime. Figure 7(a) shows the current at $E_g = -U/2 = -12.5\, k_B T$ calculated with 2vN and 1vN methods. Since level broadening is not included in the first-order method the peaks are too high and narrow.

More interesting, we see that the current minimum has been shifted away from degeneracy. Comparing with the noninteracting results of Fig. 2, where the dip is found at $\Delta E = 0$ at $E_g = \pm U/2$, one draws the conclusion that the shift is related to the finite charging energy U. We will argue that this shift has three origins:

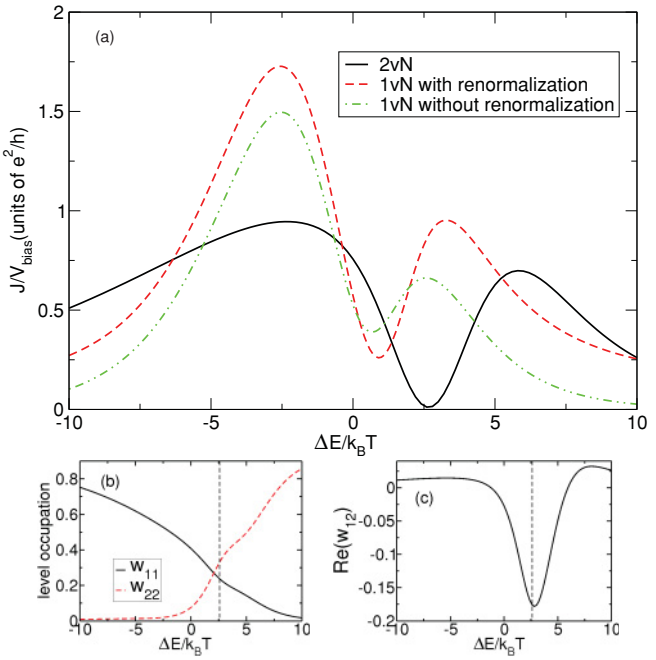

FIG. 7. (Color online) (a) The current through the two-level quantum dot calculated with 2vN and 1vN formalisms, with and without renormalization of the energy levels, at $\Gamma_1 = 4\, k_B T$, $U = 25\, k_B T$, $E_g = -U/2$, $a = 0.5$, and $V_{\text{bias}} = 2.5\, k_B T$. As the broadening is not included the first-order method overestimates the peak height but underestimates the shift away from degeneracy of the conductance dip. (b) and (c) show the corresponding occupations and real part of the coherence calculated with the 2vN formalism. The vertical dashed line marks the location of the conductance minimum.

(i) A small part of the shift originates from a first-order level renormalization and a bias-induced anticrossing between the levels, as can be seen from the slightly different dip location of the two 1vN curves in Fig. 7(a). The first-order simulations not including these effects also show a shift; however, slightly smaller. This suggests that there are additional mechanisms producing the shift. The bias-induced anticrossing is further discussed in Sec. VII in connection with the population inversion.

(ii) The main shift within the first-order approach can be attributed to the asymmetry in couplings, which has to be compensated by different spectral weights in order to allow for full canceling of the individual channels. As discussed in Ref. 11 the spectral density of each state is divided among two peaks, situated at E and $E+U$. Increasing the occupation of one level results in a shift in the spectral function of the other level toward the upper peak at $E+U$. At $E_g=-U/2$ the upper peak is far from the Fermi level of the leads and does not contribute to the transport through the dot. In order for the stronger or weaker coupled level (i.e., levels 1 or 2 for $|a|<1$) to have lower or higher spectral weight at the Fermi energy, the weaker coupled level must have a higher occupation. This is naturally the case if this level is lower in energy; thus at $E_g\approx -U/2$ the current minimum requires a positive ΔE, cf. Eq. (5). This effect is reduced for increased bias. For $f_L(E_1)=f_L(E_2)=1$ and $f_R(E_1)=f_R(E_2)=0$, complete conductance suppression can be found at degeneracy due to an increased occupation of the weakly coupled level, as discussed below.

(iii) Comparing the first- and second-order methods it is clear that the inclusion of broadening of the levels increases the shift of the conductance dip. It is well known that in a broadened level the low-energy part of the spectral density is mostly occupied.[43] Because of the Coulomb interaction this results in a significantly higher occupation of the strongly coupled level at level degeneracy; see Fig. 7(b) and Refs. 12 and 13. To compensate, the minimum is shifted so that the strongly coupled level has a higher energy than the weakly coupled. Because of the level broadening one cannot expect the two levels to contribute equally to the current away from the degeneracy point. As the levels are equally far from the bias window, the broader level will have a stronger contribution if the occupations of the two levels are equal. Thus the minimum can be found for values of ΔE such that the occupation of the weakly coupled level is slightly higher, in agreement with Fig. 7(b). In the regime $|E_g|>U/2$ Coulomb interaction is of minor importance but the dip is still found where the occupation of the weakly coupled level is higher, to compensate for the larger broadening of the strongly coupled level. This implies the strong shift outside the Coulomb-blockade region, as obtained by NEGF.

Note that the above explanation holds not only in the sequential but also in the cotunneling regime $-U/2<E_g<U/2$, but the argument has to be reversed for $E_g>0$, where the current is mainly carried by holes through the doubly occupied states. At electron-hole symmetry the singly and doubly occupied levels have the same distance from the bias window, which results in minimal conductance at level degeneracy.

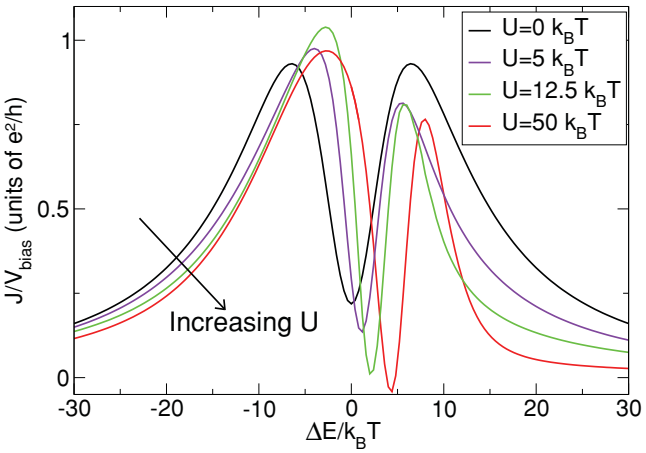

FIG. 8. (Color online) The conductance of the two-level quantum dot at $\Gamma_1=5\,k_BT$, $a=0.5$, $V_{\rm bias}=2.5\,k_BT$, and $E_g=-U/2$. Increasing U leads to a shift of the conductance minimum toward positive ΔE, where the less coupled state is lower in energy.

In the sequential tunneling regime the canceling of the different current paths through the dot is related to coherence between the levels. For the couplings considered here we concluded in Sec. V that a negative real part of the coherence led to a decreased current. It is thus not surprising that Fig. 7(c) shows that the current minimum coincides with a minimum in the real part of the coherence.

The relation between the charging energy and the shift of the dip can be better understood by studying the current at $E_g=-U/2$ for different values of U. This is done in Fig. 8 for $V_{\rm bias}=2.5\,k_BT$. Here $U=0$ corresponds to electron-hole symmetry and the conductance suppression is not complete because of the finite bias. As the charging energy increases, the current will mainly flow through the singly occupied dot states. As predicted above, this results in a shift of the conductance dip toward lower energy of the weakly coupled state. Because of the different occupations the current through the two levels cancel for larger U, resulting in a strong conductance suppression. Thus a larger U results in stronger conductance suppression at the dip, in agreement with Fig. 8.

We now focus on the case of higher bias. When both levels are in the bias window and $k_BT\ll V_{\rm bias}$ the current can be calculated using the first-order results. Here it is important whether the charging energy is dominating over bias or not. For $U\ll V_{\rm bias}$, i.e., in the ultra-high-bias limit [Fig. 1(c)], both the singly and doubly occupied levels are inside the bias window and the current can be calculated using Eq. (A17),

$$J=\frac{\Gamma_1}{\hbar}\frac{(1+a^2)\left[(1-a^2)^2+(E_1-E_2)^2/\Gamma_1^2\right]}{2\left[(1+a^2)^2+(E_1-E_2)^2/\Gamma_1^2\right]}, \qquad (25)$$

in agreement with Ref. 16. The dip is found at $E_1=E_2$ but the suppression is not complete. (Note that this result corresponds to electron-hole symmetry.)

For $U\to\infty$, i.e. the high-bias case [Fig. 1(b)], the doubly occupied state will be empty and the current is given by

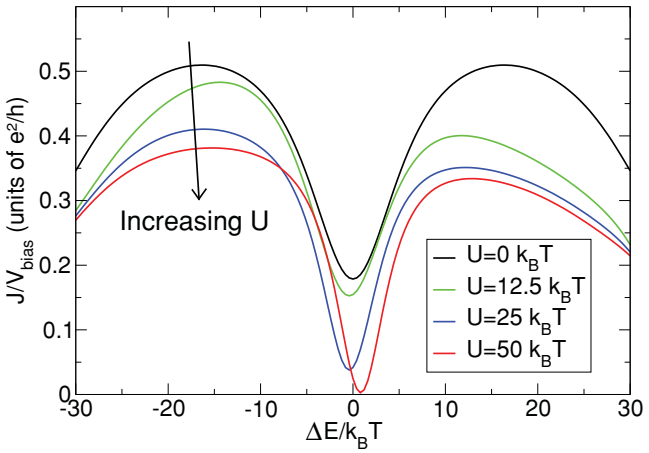

FIG. 9. (Color online) The conductance of the two-level quantum dot at $\Gamma_1 = 5\,k_BT$, $a = 0.5$, $V_{\rm bias} = 30\,k_BT$, and $E_g = -U/2$. As predicted, increasing U leads to reduced conductance at level degeneracy.

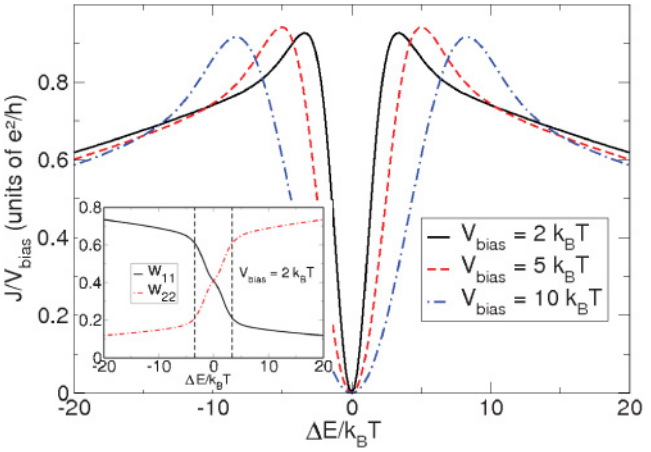

FIG. 10. (Color online) Conductance at $E_g = 0$ of the two-level quantum dot as a function of the level splitting for different values of $V_{\rm bias}$. The insert shows the occupation of the two single-particle levels for $V_{\rm bias} = 2\,k_BT$, with the vertical dashed lines marking the location of the current peaks. The parameters are given by $a = 1$, $\Gamma_1 = 20\,k_BT$, and $U = 100\,k_BT$.

Eq. (A22),

$$J = \frac{\Gamma_1}{\hbar}\frac{(1+a^2)(E_1-E_2)^2/\Gamma_1^2}{(1+a^2)^2+3(E_1-E_2)^2/\Gamma_1^2}, \tag{26}$$

again in agreement with Ref. 16. We note that the current is zero at $E_1 = E_2$. This can be explained intuitively[27,28]: At degeneracy we are free to work in any linear combination of our original single-particle basis. Especially we can choose a basis such that one level, $\Psi_{\rm filled} = \alpha\Psi_1 + \beta\Psi_2$, is completely decoupled from the lead with the low chemical potential. This level will always be occupied because of the high bias. However, the other level cannot be occupied as $U \to \infty$. As a result neither level can carry any current through the dot, as seen for $U = 50\,k_BT$ in Fig. 9. It is evident that if level 1 is more strongly coupled than level 2, then $\beta > \alpha$, implying that the weakly coupled level has a higher occupancy, as discussed above.

At high bias, as in Fig. 9, the conductance minimum can be found close to level degeneracy in agreement with Eqs. (25) and (26). The symmetry with respect to mirroring in $\Delta E = 0$, for $U = 0$ is broken by a finite U. Comparing Figs. 8 and 9 shows that increasing the bias increases the width of the dip and broadens the peaks.

In this section the current suppression away from electron-hole symmetry was investigated. Since the levels were close to the bias window, sequential tunneling was important, and different parity of the two levels was essential for the suppression. At finite bias, the suppression was not complete unless the levels had the same coupling strength. However, a finite Coulomb interaction shifted the dip away from degeneracy and resulted in a stronger suppression. This shift, not previously discussed in the literature, was studied in detail. Three origins for the shift were found: (i) a renormalization of the energy levels, (ii) a shift required to give the weakly coupled level a higher occupation that reduces the spectral weight of the singly occupied state for the other level in the case of Coulomb repulsion, and (iii) a shift related to the broadening of the levels. Furthermore, in the high-bias regime, Fig. 1(b), there was complete current suppression at the degeneracy point.

VII. CURRENT PEAKS AND POPULATION INVERSION

In this section we change the focus from the dip to the surrounding current peaks. In the limit of zero bias and zero temperature and $w_{00} = w_{dd} = 0$, it was shown in Ref. 14 that, for the couplings of Eq. (6), the peaks correspond to a difference in occupation of $|w_{11} - w_{22}| = 0.5$. To verify if the 2vN method can reproduce these results we must go to the regime $\Gamma \gg V_{\rm bias}, k_BT$, i.e., to the boundary of the region of validity of the 2vN method. To reduce the possible occurrence of negative currents we use couplings with $a = 1$, where the current is inherently zero at degeneracy. The result of the simulations is shown in Fig. 10, where the black curve corresponds to low bias, $V_{\rm bias} = 2\,k_BT$. Closer examination reveals that the peaks are located at $\Delta E = \pm 3.4\,k_BT$ where $|w_{11} - w_{22}| \approx 0.4$, in good agreement with the analytical prediction. It is not surprising that the difference in occupation is smaller than predicted since there is also a finite probability that the dot is empty or doubly occupied.

A more surprising result is found when the occupations for higher values of $V_{\rm bias}$ are studied; see Fig. 11. This is a regime of validity for the 2vN method due to the increased bias. It should be pointed out that the regime described here, where the upper state is far below the chemical potentials, cannot be studied in pure second-order perturbation in Γ. Such methods do not include mechanisms for emptying the upper state.[44,45] On each side of the level degeneracy there is a region of population inversion, i.e., the upper level has a higher occupation. This population inversion has not previously been investigated for our system; however, a similar heating of single-electron transistors due to inelastic cotunneling processes was discussed in Ref. 46. The 2vN simulation for the single-level dot with spin, where a magnetic field splits both spin directions (Anderson model, not shown) reveals no population inversion between the two spin levels. This suggests that the coherence between the two orbital levels is essential for the inversion. The coherence simply means that an electron can be in a superposition of the two states, which results from

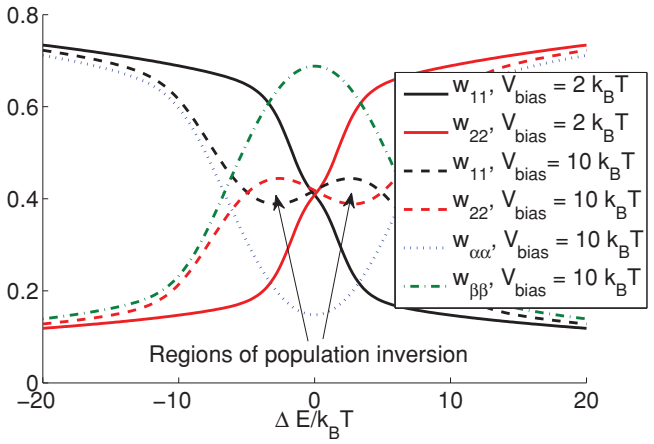

FIG. 11. (Color online) Occupation of the two single-particle levels for different values of $V_{\rm bias}$. Around degeneracy a region of population inversion can be found. The parameters are given by $a = 1$, $\Gamma_1 = 20\,k_BT$, and $U = 100\,k_BT$. The population inversion in the diagonal basis ($|\alpha\rangle$, $|\beta\rangle$) is calculated using Ω from Eq. (27).

the overlap between the dot levels introduced by the couplings to the leads. For the level configuration of Fig. 11 the dot can, as a good approximation, be considered to be singly occupied, which means that the Schrieffer–Wolff transformation of Sec. IV can be used to evaluate the overlap. As noted in Sec. IV, in connection with Eq. (16), the contribution to the overlap from state E_k in the leads is proportional to $c^\dagger_{kL}c_{kL} - c^\dagger_{kR}c_{kR} \Longrightarrow f_L(E_k) - f_R(E_k)$, which vanishes in the low-bias limit. As a result the coherence and the overlap between the dot states vanish. However, a finite bias results in an effective overlap between the two states. Replacing the sums with integrals and using the notation of Eq. (5), one arrives at the following expression for the anticrossing Ω,

$$\Omega = \frac{1}{2}at^2\left(\ln\left|\frac{V_{\rm bias}-U-\Delta E}{V_{\rm bias}+U+\Delta E}\right| + \ln\left|\frac{V_{\rm bias}-U+\Delta E}{V_{\rm bias}+U-\Delta E}\right|\right) \tag{27}$$

in the additional term of the dot Hamiltonian given by $\Omega(d_1^\dagger d_2 + d_2^\dagger d_1)$. We have assumed $k_BT = 0$. As long as $\Delta E < U$, which always is the case if Eq. (27) is valid, Ω is negative for $V_{\rm bias} > 0$. For small bias $V_{\rm bias} < \Delta E$ the anticrossing vanishes. This is expected as inelastic processes where the state of the dot is changed are possible only as long as $V_{\rm bias} > \Delta E$. To investigate the effect of this anticrossing we diagonalize the dot Hamiltonian. The resulting eigenvalues and eigenvectors are given by

$$E_{\alpha/\beta} = \tfrac{1}{2}(E_1 + E_2 \mp \sqrt{\Delta E^2 + 4\Omega^2}), \tag{28}$$

$$\begin{aligned} |\alpha\rangle &= x_{\alpha 1}\,|1\rangle + x_{\alpha 2}\,|2\rangle\,, \\ |\beta\rangle &= x_{\beta 1}\,|1\rangle + x_{\beta 2}\,|2\rangle\,, \end{aligned} \tag{29}$$

where the coefficients are given by

$$\begin{aligned} x_{\alpha 1} &= \frac{N_\alpha}{2\Omega}(\Delta E - \sqrt{\Delta E^2 + 4\Omega^2}), \quad x_{\alpha 2} = N_\alpha, \\ x_{\beta 1} &= \frac{N_\beta}{2\Omega}(\Delta E + \sqrt{\Delta E^2 + 4\Omega^2}), \quad x_{\alpha 2} = N_\beta, \end{aligned} \tag{30}$$

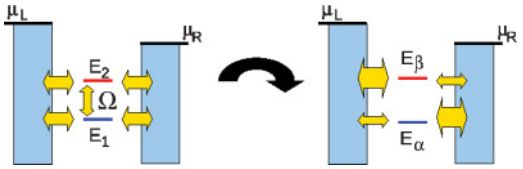

FIG. 12. (Color online) The finite bias induces an anticrossing Ω between the two original states. Diagonalizing the dot Hamiltonian results in the upper state being strongly coupled to the lead with high chemical potential, while the lower state is strongly coupled to the lead with low chemical potential.

respectively, with N_α and N_β being normalization constants. Clearly we always have $E_\alpha < E_\beta$. The new eigenstates also get new effective couplings:

$$\begin{aligned} t_{L\alpha} &= (x_{\alpha 1}t - x_{\alpha 2}at), \quad t_{R\alpha} = (x_{\alpha 1}t + x_{\alpha 2}at), \\ t_{L\beta} &= (x_{\beta 1}t - x_{\beta 2}at), \quad t_{R\beta} = (x_{\beta 1}t + x_{\beta 2}at). \end{aligned} \tag{31}$$

Because of $\Omega < 0$ both coefficients $x_{\alpha 1}$ and $x_{\alpha 2}$ of the lower eigenstate $|\alpha\rangle$ have the same sign. Combined with the difference in parity of our two original states this results in a weak coupling of $|\alpha\rangle$ to the left lead, i.e., the lead with high chemical potential, and a strong coupling to the right lead. In the same way $|\beta\rangle$ couples strongly to the left and weakly to the right; see Fig. 12. The population inversion is real in the sense that it is present in the diagonal basis of the dot ($|\alpha\rangle$ $|\beta\rangle$); see Fig. 11. It might at first seem surprising that the population inversion is so large. For $V_{\rm bias} = 10\,k_BT$ in Fig. 11 we have $\Omega \approx 4\,k_BT$ over the entire range of ΔE. The detuning $E_\beta - E_\alpha = 2\Omega$ at $E_1 - E_2 = 0$, i.e., it is almost the size of $V_{\rm bias}$, and yet a strong population inversion is observed. The cause for this population inversion is inelastic processes driving a current from left to right by filling the state $|\beta\rangle$ and emptying $|\alpha\rangle$. Because of the asymmetric couplings of the ($|\alpha\rangle$,$|\beta\rangle$) basis, such processes are very strong. The populations of Fig. 11 in the ($|\alpha\rangle$,$|\beta\rangle$) basis are calculated assuming Ω given by Eq. (27). Deviations from single occupation of the quantum dot, because of the broadening of the dot levels and the finite bias, cause slightly different values of Ω. However, at $\Delta E = 0$, $|\alpha\rangle$ and $|\beta\rangle$ are the symmetric and antisymmetric combinations of $|1\rangle$ and $|2\rangle$, respectively, independent of Ω. Therefore, the population inversion is independent of Ω at $\Delta E = 0$. For higher bias this results in populations close to $w_{\alpha\alpha} = 0$ and $w_{\beta\beta} = 1$. In the limit $V_{\rm bias} \to \infty$, it cannot be considered as a population inversion since Ω vanishes in this limit, resulting in $E_\alpha = E_\beta$.

When $\Delta E < 0$, i.e., $E_1 < E_2$, $|\alpha\rangle$ is mainly composed of the original state $|1\rangle$, while $|\beta\rangle$ is mainly composed of $|2\rangle$. For $\Delta E > 0$ the situation is the reverse. Thus, it is always the case that the upper state $|\beta\rangle$, which couples strongly to the left, is mainly composed of the upper state in the original basis. This explains the observed population inversion in our original basis. A negative bias results in $\Omega > 0$, which leads to a strong coupling of $|\alpha\rangle$ to the left. However, for a negative bias the left lead has a low chemical potential. Thus the explanation holds also for negative bias.

The $k = k'$ terms of Eq. (16) are present also in first-order perturbation in dot-lead couplings. We have seen that the real

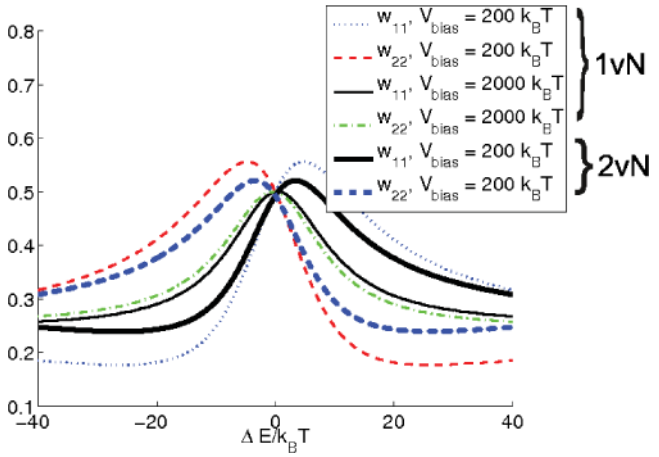

FIG. 13. (Color online) Populations calculated with the 1vN and 2vN methods. Couplings and charging energy are given by $\Gamma_1 = 5\,k_BT$ and $U = 100\,k_BT$, respectively.

part of the sum (or integral in the continuous limit) over $k = k'$ gives rise to the population inversion. We thus expect to see population inversion also in first-order simulations if the real part is included. However, first-order perturbation theory cannot be applied to the cotunneling regime where Eq. (16) is valid. We instead investigate the ultra-high-bias regime where all states are inside the bias window. Equation (A2) can be solved including the real part of the sums. The result is shown in Fig. 13, where also the result of a 2vN simulation is shown as comparison. One observes that, as the bias is increased, which means that the real parts of the sums become smaller, the occupations approach the infinite-bias result of Eq. (A15). It is evident that the broadening results in a smaller population inversion. We can therefore not completely rule out the possibility that the population inversion is an effect of neglecting higher-order couplings. As the inversion is present also at very high bias, where the contribution from higher-order terms is small, we believe, however, that it is a real effect. Since it is the real part of of the sums of Eq. (A2) that is responsible for the renormalization one would not expect to see any population inversion when these are neglected. Indeed, already at $V_{\text{bias}} = 200\,k_BT$ one finds that the results of such simulations are indistinguishable from Eq. (A15). These results are therefore not shown in Fig. 13.

The population inversion is in fact related to the conductance peaks, by increasing the elastic cotunneling. Let us assume that $E_2 > E_1$ so that $w_{22} > w_{11}$. Then in Eq. (18) the elastic processes with $d_2^\dagger d_2$ will dominate. If the levels are placed as in Fig. 1(a), then $E_k - (E_1 + U)$ and $-(E_k - E_2)$ are both positive and there is constructive interference between these tunneling processes. Put simply, the population inversion activates elastic processes through the states close to the bias window, i.e., processes that contribute strongly to the current. Furthermore, the elastic processes have the same phase and interfere constructively. For large detuning, ΔE, the coherence decreases and as a result the occupation of the upper level will decrease. Increased temperature, which also results in a lower coherence and a related decrease in population inversion, also leads to decreased peak height. This scenario describes the formation of the conductance peaks at finite bias.

Finally we would like to point out the experimental significance of the results presented in this section. By embedding the quantum dot in, e.g., a microwave cavity the dot can be connected to a photon mode. Because of the population inversion this couping might lead to stimulated emission of photons, i.e., a maser is formed. Previously it has been suggested that such a population inversion can be reached in double quantum dot systems, where the inversion results from an asymmetric couping of the dots to left and right leads.[47] The results of this section suggest that an increased bias will modify the dot Hamiltonian of two-level quantum dots so that such couplings are achieved, as long as the original dot levels have different parity. The difference in parity guarantees a nonzero dipole element between the dot levels. One would expect the dipole element to be larger in two-level quantum dots than in double quantum dots because of the spatial overlap of the two states. This suggests an increased observability of population inversion in two-level quantum dots.

VIII. CONCLUDING REMARKS

A thorough study of the transport through spinless two-level quantum dots has been presented. Regimes not previously studied in the presence of cotunneling, such as the regimes of finite bias and temperature, as well as the transport away from electron-hole symmetry, was studied. To present a coherent picture of the transport through the system, comparison with previously derived results were made.

Close to degeneracy a suppression of the current was found, while a slight detuning of the energy levels resulted in current peaks. This resulted in a canyon of current suppression cutting through both the sequential-tunneling and cotunneling regime. Different mechanism for the suppression were found in the different regimes. In the Coulomb-blockade region an intuitive explanation to the suppression was presented in the low-energy regime, in terms of canceling of different tunneling processes because of equal occupation of the two levels. In the high-bias limit with infinite charging energy a complete suppression was found since the electron was trapped in a nonconducting state, preventing any transport. These two mechanisms for the suppression are independent of the lead-dot couplings. When neither of the above mechanism was present, different parity of the two dot levels had to be assumed to achieve current suppression. For such couplings the canyon was found close to degeneracy in all four cases (high and low bias, strong and weak couplings), independent of the level positions, albeit the current did not always entirely drop to zero.

To quantify the current suppression, simulations were performed using the second-order von Neumann technique. In the regime where the lead-dot couplings dominate over temperature and applied bias, i.e., cotunneling processes contribute strongly to the current, a strong suppression was observed both in the sequential and the cotunneling regime, assuming different parity of the two levels. For weaker couplings, where cotunneling could be neglected, only partial suppression was observed in agreement with analytical results.

Away from the electron-hole symmetry point a shift of the conductance dip was observed. The shift was shown to have three origins: (i) a renormalization of the energy levels, (ii) a shift required to give the weakly coupled level a higher occupation, and (iii) a shift related to the broadening of the levels.

Finally the conductance peaks were investigated. The peaks were found to be intimately related to an increased occupation of the upper level. The increased population resulted from the bias-induced anticrossing between the two orbital levels. Sufficiently high bias resulted in an anticrossing large enough to cause population inversion.

ACKNOWLEDGMENTS

We would like to thank Henrik Nilsson, Hongqi Xu and Christian Bergenfeldt for many discussions. Financial support from the Swedish Research Council (VR) is gratefully acknowledged.

APPENDIX A: CURRENT IN THE FIRST-ORDER VON NEUMANN APPROACH

In this Appendix we will derive expressions for the current assuming that the broadening can be neglected. The results are thus of first order in Γ. In the von Neumann formalism the Markov approximation is made within the Schrödinger picture, as compared with the Redfield method where the Markov limit is taken in the interaction picture. This results in slightly different results when the levels are nondegenerate.[40]

Equation (4) defines $t_{n\ell}(k)$ as the coupling of a single particle state n to state k in lead ℓ. The couplings of the corresponding many-particle states are given by

$$T_{ba\ell}(k) = \sum_n t_{n\ell}(k)\langle b|d_n^\dagger|a\rangle, \tag{A1}$$

where $|a\rangle$ and $|b\rangle$ are dot states. We use the convention that the many-particle state b contains one more dot electron than a and so on. Assuming energy-independent couplings, $T_{ba\ell}(k) = T_{ba\ell}$, the equation of motion for the reduced density matrix is in the first-order von Neumann method given by[39]:

$$\begin{aligned}
i\hbar\frac{d}{dt}w_{bb'} &= (E_b - E_{b'})w_{bb'} \\
&+ \sum_{a,k\ell} T_{ba\ell}\frac{\sum_{a'} w_{aa'}T^*_{b'a'\ell}f_k - \sum_{b''} T^*_{b''a\ell}w_{b''b'}(1-f_k)}{E_k - E_{b'} + E_a - i0^+} - \sum_{a,k\ell}\frac{\sum_{a'} T_{ba'\ell}w_{a'a}f_k - \sum_{b''} w_{bb''}T_{b''a\ell}(1-f_k)}{E_k - E_b + E_a + i0^+}T^*_{b'a\ell} \\
&+ \sum_{c,k\ell} T^*_{cb\ell}\frac{\sum_{b''} T_{cb''\ell}w_{b''b'}f_k - \sum_{c'} w_{cc'}T_{c'b'\ell}(1-f_k)}{E_k - E_c + E_{b'} + i0^+} - \sum_{c,k\ell}\frac{\sum_{b''} w_{bb''}T^*_{cb''\ell}f_k - \sum_{c'} T^*_{c'b\ell}w_{c'c}(1-f_k)}{E_k - E_c + E_b - i0^+}T_{cb'\ell},
\end{aligned} \tag{A2}$$

where f_k is the Fermi distribution.

Going to the continuum limit one replaces the sums over k with integrals. The real parts of the integrals constitute a renormalization of the energy levels. However, the results of this appendix are applied either to electron-hole symmetry or to the high or high-bias or ultra-high-bias case. In these situations the renormalization vanishes, and for the couplings of Eqs. (6) the stationary 1vN equations read, for the vacuum state $b = 0, b' = 0$,

$$\begin{aligned}
&- w_{00}\{f_L(E_1) + f_R(E_1) + a^2[f_L(E_2) + f_R(E_2)]\} + w_{11}\{2 - f_L(E_1) - f_R(E_1)\} \\
&+ a^2 w_{22}\{2 - f_L(E_2) - f_R(E_2)\} + a\mathcal{R}\{w_{12}\}\{f_L(E_1) + f_L(E_2) - f_R(E_1) - f_R(E_2)\} = 0;
\end{aligned} \tag{A3}$$

for the single-particle state $b = 1, b' = 1$,

$$\begin{aligned}
&w_{00}\{f_L(E_1) + f_R(E_1)\} - w_{11}\{2 - f_L(E_1) - f_R(E_1) + [f_L(E_2+U) + f_R(E_2+U)]a^2\} \\
&+ a^2 w_{dd}\{2 - f_L(E_2+U) - f_R(E_2+U)\} - a\mathcal{R}\{w_{12}\}\{f_L(E_1) + f_L(E_2+U) - f_R(E_1) - f_R(E_2+U)\} = 0;
\end{aligned} \tag{A4}$$

for the other single-particle state $b = 2, b' = 2$,

$$\begin{aligned}
&a^2 w_{00}\{f_L(E_2) + f_R(E_2)\} - w_{22}\{[2 - f_L(E_2) - f_R(E_2)]a^2 + f_L(E_1+U) + f_R(E_1+U)\} \\
&+ w_{dd}\{2 - f_L(E_1+U) - f_R(E_1+U)\} - a\mathcal{R}\{w_{12}\}\{f_L(E_2) + f_L(E_1+U) - f_R(E_2) - f_R(E_1+U)\} = 0;
\end{aligned} \tag{A5}$$

and for the coherence $b = 1, b' = 2$, ($b = 2, b' = 1$ gives the same information since $w_{21} = w_{12}^*$);

$$\begin{aligned}
&- ia\frac{w_{00}}{2}\{f_L(E_1) + f_L(E_2) - f_R(E_1) - f_R(E_2)\} - ia\frac{w_{dd}}{2}\{f_L(E_1+U) + f_L(E_2+U) - f_R(E_1+U) - f_R(E_2+U)\} \\
&- ia\frac{w_{11}}{2}\{f_L(E_1) - f_R(E_1) + f_L(E_2+U) - f_R(E_2+U)\} - ia\frac{w_{22}}{2}\{f_L(E_2) - f_R(E_2) + f_L(E_1+U) - f_R(E_1+U)\}
\end{aligned}$$

$$-\mathrm{i}\frac{w_{12}}{2}[2-f_L(E_2)-f_R(E_2)+f_L(E_2+U)+f_R(E_2+U)$$
$$+a^2(2-f_L(E_1)-f_R(E_1)+f_L(E_1+U)+f_R(E_1+U))]+\frac{E_1-E_2}{\Gamma_1}w_{12}=0. \tag{A6}$$

The equation for $b=d$, $b'=d$ (doubly occupied state) does not provide any new information. One must instead use the normalization

$$w_{00}+w_{11}+w_{22}+w_{dd}=1. \tag{A7}$$

At $E_1=E_2=-U/2$, where $w_{00}=w_{dd}$, the equations of motion are symmetric in the two levels. This results in an equal population of the two states. Furthermore the (E_1-E_2) term of Eq. (A6) disappears, implying that the coherence is real, as remarked in Sec. V.

Once the system of equations has been solved, the current can be calculated with[39]

$$J=\frac{\Gamma_1}{\hbar}\{w_{00}[f_L(E_1)+f_L(E_2)a^2]-w_{11}[1-f_L(E_1)]+w_{11}f_L(E_2+U)a^2-w_{22}[1-f_L(E_2)]a^2+w_{22}f_L(E_1+U)$$
$$-w_{dd}[1-f_L(E_1+U)+[1-f_L(E_2+U)]a^2]+a\mathcal{R}\{w_{12}\}[2-f_L(E_1)-f_L(E_2)+f_L(E_1+U)+f_L(E_2+U)]\}. \tag{A8}$$

We first consider the ultra-high-bias limit, i.e., $f_L(E_1)=f_L(E_2)=f_L(E_1+U)=f_L(E_2+U)=1$ and $f_R(E_1)=f_R(E_2)=f_R(E_1+U)=f_R(E_2+U)=0$. Inserting these occupations in Eqs. (A3)–(A6) we obtains

$$-w_{00}(1+a^2)+w_{11}+a^2w_{22}+2a\mathcal{R}\{w_{12}\}=0, \tag{A9}$$
$$w_{00}-w_{11}(1+a^2)+a^2w_{dd}-2a\mathcal{R}\{w_{12}\}=0, \tag{A10}$$
$$a^2w_{00}-w_{22}(1+a^2)+w_{dd}-2a\mathcal{R}\{w_{12}\}=0, \tag{A11}$$
$$-\mathrm{i}aw_{00}-\mathrm{i}aw_{11}-\mathrm{i}aw_{22}-\mathrm{i}aw_{dd}-\mathrm{i}(1+a^2)w_{12}+\frac{E_1-E_2}{\Gamma_1}w_{12}=0. \tag{A12}$$

The imaginary part of w_{12} occurs in only the last equation and can easily be expressed in terms of the real part of w_{12}:

$$\mathcal{I}\{w_{12}\}=-\frac{(E_1-E_2)\mathcal{R}\{w_{12}\}}{\Gamma_1(1+a^2)}. \tag{A13}$$

Equation (A12) can then be rewritten as

$$aw_{00}+aw_{11}+aw_{22}+aw_{dd}+\left[1+a^2+\frac{(E_1-E_2)^2}{\Gamma_1(1+a^2)}\right]\mathcal{R}\{w_{12}\}=0. \tag{A14}$$

Solving for the occupations one finds

$$w_{11}=w_{22}=\frac{1}{4}+\frac{a^2}{(1+a^2)^2+(E_1-E_2)^2/\Gamma_1^2}, \tag{A15}$$

as noted in Sec. VII. Using Eq. (A8) the current can be calculated as

$$J=\frac{\Gamma_1}{\hbar}[w_{00}(1+a^2)+w_{11}a^2+w_{22}+2a\mathcal{R}\{w_{12}\}]. \tag{A16}$$

Solving Eqs. (A9)–(A12) results in

$$J=\frac{\Gamma_1}{\hbar}\frac{(1+a^2)\left[(1-a^2)^2+(E_1-E_2)^2/\Gamma_1^2\right]}{2\left[(1+a^2)^2+(E_1-E_2)^2/\Gamma_1^2\right]}. \tag{A17}$$

It is easy to show that the conductance minimum is found at $E_1=E_2$ where, for a general value of the bias, the current is given by Eq. (22).

We next turn to the high-bias limit $U=\infty$, i.e., $f_L(E_1)=f_L(E_2)=1$ and $f_R(E_1)=f_R(E_2)=f_R(E_1+U)=f_R(E_2+U)=f_L(E_1+U)=f_L(E_2+U)=0$. Here it trivially follows from the equation for $b=b'=d$ that w_{dd} is zero. Furthermore Eq. (A3) is redundant. The remaining equations for the occupations are given by

$$w_{00}-w_{11}-a\mathcal{R}\{w_{12}\}=0, \tag{A18}$$
$$a^2w_{00}-a^2w_{22}-a\mathcal{R}\{w_{12}\}=0, \tag{A19}$$
$$-\mathrm{i}aw_{00}-\mathrm{i}a\frac{w_{11}}{2}-\mathrm{i}a\frac{w_{22}}{2}-\mathrm{i}\frac{w_{12}}{2}(1+a^2)+\frac{E_1-E_2}{\Gamma_1}w_{12}=0. \tag{A20}$$

From Eq. (A20) $\mathcal{I}\{w_{12}\}$ can be determined

$$\mathcal{I}\{w_{12}\} = -\frac{2(E_1 - E_2)\mathcal{R}\{w_{12}\}}{\Gamma_1(1+a^2)}. \tag{A21}$$

Thus in the case $U = \infty$ the current is given by

$$J = \frac{\Gamma_1}{\hbar} w_{00}(1+a^2) = \frac{\Gamma_1}{\hbar} \frac{(1+a^2)(E_1 - E_2)^2/\Gamma_1^2}{(1+a^2)^2 + 3(E_1 - E_2)^2/\Gamma_1^2}. \tag{A22}$$

Once again the conductance minimum is at degeneracy but for $U = \infty$ there is complete conductance suppression independent of the relative coupling strength a, in agreement with Refs. 27 and 28.

APPENDIX B: RENORMALIZATION OF THE DOT LEVELS FROM THE SCHRIEFFER–WOLFF TRANSFORMATION

In this Appendix we give the derivation of Eq. (17). The renormalization, given by the $k = k'$ terms, reads

$$\begin{aligned}\hat{H}_{\text{renorm}} = 2\left(\sum_k \frac{-t^2}{E_k - E_1}\left(1 - \frac{1}{2}(c_{kL}^\dagger c_{k_L} + c_{kR}^\dagger c_{k_R})\right) + \sum_k \frac{a^2 t^2}{E_k - (E_2 + U)}\frac{1}{2}(c_{kL}^\dagger c_{k_L} + c_{kR}^\dagger c_{k_R})\right) d_1^\dagger d_1 \\ + 2\left(\sum_k \frac{-a^2 t^2}{E_k - E_2}\left(1 - \frac{1}{2}(c_{kL}^\dagger c_{k_L} + c_{kR}^\dagger c_{k_R})\right) + \sum_k \frac{t^2}{E_k - (E_1 + U)}\frac{1}{2}(c_{kL}^\dagger c_{k_L} + c_{kR}^\dagger c_{k_R})\right) d_2^\dagger d_2,\end{aligned}$$

where the factor of 2 accounts for the Hermitian conjugate in Eq. (16). One sees that the sums are actually logarithmically divergent, which of course seems like a problem at first sight. However, a common renormalization of the two levels is just a shift of the zero point in the Hamiltonian that can be neglected. The physically interesting quantity is the difference in renormalization of the two levels. We first assume that level 2 is fixed, transferring the whole renormalization to level 1. Replacing the operators with their expectation values $c_{kl}^\dagger c_{k_l} \approx \langle c_{kL}^\dagger c_{k_L}\rangle = f_l(E_k) = f(E_k)$, in the low-bias limit, and using $\Gamma_1(E) = 2\pi \sum_k t^2 \delta(E_k - E)$ and a constant density of states, the renormalization is given by

$$\begin{aligned}\hat{H}_{\text{renorm}} = \frac{\Gamma_1}{\pi}\left(-\mathcal{P}\left\{\int_{-\infty}^{\infty} dE_k \frac{1}{E_k - E_1}(1 - f(E_k))\right\} - \mathcal{P}\left\{\int_{-\infty}^{\infty} dE_k \frac{1}{E_k - (E_1 + U)} f(E_k)\right\}\right. \\ \left. + a^2\mathcal{P}\left\{\int_{-\infty}^{\infty} dE_k \frac{1}{E_k - E_2}(1 - f(E_k))\right\} + a^2\mathcal{P}\left\{\int_{-\infty}^{\infty} dE_k \frac{1}{E_k - (E_2 + U)} f(E_k)\right\}\right) d_1^\dagger d_1,\end{aligned} \tag{B1}$$

with $\mathcal{P}$ denoting the principal value of the integral. Inserting $f(E_k) = 1$ for $E_k < 0$ and $f(E_k) = 0$ for $E_k > 0$, corresponding to the low-temperature limit, and adding the constant term $a^2 \ln|E_2/(E_2 + U)|$, we obtain Eq. (17)

$$\hat{H}_{\text{renorm}} = \frac{\Gamma_1}{\pi}\left(\ln\left|\frac{E_1}{E_1 + U}\right| d_1^\dagger d_1 + a^2 \ln\left|\frac{E_2}{E_2 + U}\right| d_2^\dagger d_2\right), \tag{B2}$$

where we have used $d_1^\dagger d_1 + d_2^\dagger d_2 = 1$, which is applicable because of the single occupation of the dot.

This expression can also be derived from the first-order Redfield, which is similar to first order von Neumann, except that the Markov limit is taken in the interaction picture, while the Schrödinger picture is used in the von Neumann method. Redfield generates an equation of motion like Eq. (A2), but with different energy denominators in the equations for the off-diagonal terms of the reduced density matrix.

---

*Present address: Department of Micro- and Nanotechnology Technical University of Denmark DTU Nanotech, Building 345 East, DK-2800 Kongens Lyngby, Denmark.

[1] S. De Franceschi, S. Sasaki, J. M. Elzerman, W. G. van der Wiel, S. Tarucha, and L. P. Kouwenhoven, Phys. Rev. Lett. **86**, 878 (2001).
[2] C. W. J. Beenakker, Phys. Rev. B **44**, 1646 (1991).
[3] S. M. Reimann and M. Manninen, Rev. Mod. Phys. **74**, 1283 (2002).
[4] C. Payette, S. Amaha, G. Yu, J. A. Gupta, D. G. Austing, S. V. Nair, B. Partoens, and S. Tarucha, Phys. Rev. B **81**, 245310 (2010).
[5] T. H. Oosterkamp, S. F. Godijn, M. J. Uilenreef, Y. V. Nazarov, N. C. van der Vaart, and L. P. Kouwenhoven, Phys. Rev. Lett. **80**, 4951 (1998).
[6] P. W. Anderson, Phys. Rev. **124**, 41 (1961).
[7] M. Pustilnik and L. Glazman, J. Phys. Condens. Matter **16**, R513 (2004).
[8] Y. Oreg and Y. Gefen, Phys. Rev. B **55**, 13726 (1997).
[9] A. Silva, Y. Oreg, and Y. Gefen, Phys. Rev. B **66**, 195316 (2002).
[10] D. I. Golosov and Y. Gefen, Phys. Rev. B **74**, 205316 (2006).
[11] J. König and Y. Gefen, Phys. Rev. B **71**, 201308 (2005).
[12] M. Sindel, A. Silva, Y. Oreg, and J. von Delft, Phys. Rev. B **72**, 125316 (2005).
[13] V. Meden and F. Marquardt, Phys. Rev. Lett. **96**, 146801 (2006).
[14] V. Kashcheyevs, A. Schiller, A. Aharony, and O. Entin-Wohlman, Phys. Rev. B **75**, 115313 (2007).

[15]H.-W. Lee and S. Kim, Phys. Rev. Lett. **98**, 186805 (2007).
[16]G. Schaller, G. Kießlich, and T. Brandes, Phys. Rev. B **80**, 245107 (2009).
[17]P. Trocha, Phys. Rev. B **82**, 125323 (2010).
[18]H. A. Nilsson, O. Karlström, M. Larsson, P. Caroff, J. N. Pedersen, L. Samuelson, A. Wacker, L.-E. Wernersson, and H. Q. Xu, Phys. Rev. Lett. **104**, 186804 (2010).
[19]H. A. Nilsson, P. Caroff, C. Thelander, M. Larsson, J. B. Wagner, L. Wernersson, L. Samuelsson, and H. Q. Xu, Nano Lett. **9**, 3151 (2009).
[20]M. T. Björk, C. Thelander, A. E. Hansen, L. E. Jensen, M. W. Larsson, L. R. Wallenberg, and L. Samuelson, Nano Lett. **4**, 1621 (2004).
[21]I. Shorubalko, A. Pfund, R. Leturcq, M. T. Borgström, F. Gramm, E. Müller, E. Gini, and K. Ensslin, Nanotechnology **18**, 044014 (2007).
[22]Y. Hu, H. O. H. Churchill, D. J. Reilly, J. Xiang, C. M. Lieber, and C. M. Marcus, Nat. Nanotechnol. **2**, 622 (2007).
[23]A. W. Holleitner, C. R. Decker, H. Qin, K. Eberl, and R. H. Blick, Phys. Rev. Lett. **87**, 256802 (2001).
[24]J. C. Chen, A. M. Chang, and M. R. Melloch, Phys. Rev. Lett. **92**, 176801 (2004).
[25]M. Sigrist, A. Fuhrer, T. Ihn, K. Ensslin, S. E. Ulloa, W. Wegscheider, and M. Bichler, Phys. Rev. Lett. **93**, 066802 (2004).
[26]P. G. Silvestrov and Y. Imry, Phys. Rev. B **75**, 115335 (2007).
[27]F. Li, X.-Q. Li, W.-M. Zhang, and S. A. Gurvitz, Europhys. Lett. **88**, 37001 (2009).
[28]M. G. Schultz and F. von Oppen, Phys. Rev. B **80**, 033302 (2009).
[29]J. N. Pedersen and A. Wacker, Phys. Rev. B **72**, 195330 (2005); Physica E **42**, 595 (2010).
[30]J. R. Schrieffer and P. A. Wolff, Phys. Rev. **149**, 491 (1966).
[31]J. König, H. Schoeller, and G. Schön, Phys. Rev. Lett. **78**, 4482 (1997).
[32]J. König, H. Schoeller, and G. Schön, Phys. Rev. B **58**, 7882 (1998).
[33]R. K. Wangsness and F. Bloch, Phys. Rev. **89**, 728 (1953).
[34]F. Bloch, Phys. Rev. **105**, 1206 (1957).
[35]A. G. Redfield, Adv. Magn. Reson. **1**, 1 (1965).
[36]C. Timm, Phys. Rev. B **77**, 195416 (2008).
[37]S. Koller, M. Grifoni, M. Leijnse, and M. R. Wegewijs, Phys. Rev. B **82**, 235307 (2010).
[38]J. König, Ph.D. thesis, University of Karlsruhe, 1998.
[39]J. N. Pedersen, B. Lassen, A. Wacker, and M. H. Hettler, Phys. Rev. B **75**, 235314 (2007).
[40]T. V. Shahbazyan and M. E. Raikh, Phys. Rev . B **49**, 17123 (1994).
[41]Y. Y. J. Jin and X. Zheng, J. Chem. Phys. **128**, 234703 (2008).
[42]D. Boese, W. Hofstetter, and H. Schoeller, Phys. Rev. B **64**, 125309 (2001).
[43]H. Bruus and K. Flensberg, *Many-Body Quantum Theory in Condensed Matter Physics* (Oxford University Press, Oxford, 2004).
[44]I. Weymann, J. König, J. Martinek, J. Barnaś, and G. Schön, Phys. Rev. B **72**, 115334 (2005).
[45]D. Becker and D. Pfannkuche, Phys. Rev. B **77**, 205307 (2008).
[46]M. A. Laakso, T. T. Heikkilä, and Y. V. Nazarov, Phys. Rev. Lett. **104**, 196805 (2010).
[47]L. Childress, A. S. Sørensen, and M. D. Lukin, Phys. Rev. A **69**, 042302 (2004).